



A prediction model for vertical-to-horizontal ratios of PGA, PGV, and 5%-damped response spectra (0.01–10 s) for Iran

Mohammad R. Zolfaghari · Atefe Darzi

Received: 8 April 2018 / Accepted: 10 May 2019 / Published online: 10 June 2019
© Springer Nature B.V. 2019

Abstract New models are developed for the prediction of vertical-to-horizontal (V/H) spectral ratios of peak ground acceleration (PGA), peak ground velocity (PGV), and 5%-damped elastic response spectra for periods ranging from 0.01 to 10 s. The models use moment magnitude, source-to-site distance, style-of-faulting (SoF), and site classification terms as independent variables. The study is based on a well-compiled Iranian ground-motion databank, consisting of 1350 (*3) three-component accelerograms generated by 370 earthquakes. Only records with known measured time-averaged shear-wave velocity in the uppermost 30 m (V_{S30}) are used for regression analyses. The presented models are valid for moment magnitude ranging from 4.5 to 7.4, distance up to 200 km, and for earthquakes with reverse and strike-slip fault mechanisms. Four alternative mathematical forms are evaluated in terms of magnitude and distance in order to find the optimal functional form for reliable prediction of V/H ratios. Out of four proposed forms, two were chosen for further investigation. The point source (hypocentral and

epicentral) as well as extended source (rupture and Joyner-Boore) distance metrics are employed to derive four models. The overall validity of the proposed models is examined by detailed residual analyses as well as comparison with some of the local and regional predictive V/H models. Our proposed models showed significant reduction in the total standard deviation across all periods. The proposed V/H models facilitate assessment of vertical components of response spectrum where horizontal component of response spectrum is known, using V/H spectral ratios as scaling factors.

Keywords Vertical-to-horizontal ground-motion model · Iran · V/H spectral ratio · PGA · PGV

1 Introduction and motivation

In recent decades, the importance of vertical ground motions in design of short-period critical structures (e.g., nuclear power plants) and lifeline systems has become a matter of debate (Bozorgnia and Campbell 2004; Gülerce and Abrahamson 2011). Several investigators examined the relationship between horizontal and vertical components of ground motions and their corresponding characteristics (e.g., Bozorgnia and Campbell 2004; Bindi et al. 2010; Edwards et al. 2011; Poggi et al. 2012). These researchers pointed out the need to enhance predictive equations for V/H spectral ratios.

The V/H spectral ratio can be estimated using independent ground-motion prediction models for vertical and horizontal components, developed from the same

Electronic supplementary material The online version of this article (<https://doi.org/10.1007/s10950-019-09836-z>) contains supplementary material, which is available to authorized users.

M. R. Zolfaghari (✉) · A. Darzi
Civil Engineering Department, K. N. Toosi University of
Technology, Tehran, Iran
e-mail: mzolafaghari@catrisks.com

A. Darzi
e-mail: adarzi@mail.kntu.ac.ir

database and mathematical models (e.g., Soghrat and Ziyaeifar 2016a; Darzi et al. 2018; Zolfaghari and Darzi 2019). However, one of the main shortcomings identified in this approach is the difficulties in computation of V/H residuals and standard deviations. Another alternative approach is to develop empirical ground-motion models for V/H ratios directly (e.g., Bozorgnia and Campbell 2016; Akkar et al. 2014; Bommer et al. 2011) in which direct determination of residuals and standard deviations for the estimated V/H ratios can be achieved. Moreover, the consistency between horizontal and vertical components is better preserved in direct V/H models than those obtained from independent horizontal and vertical ground-motion models (Akkar et al. 2014).

Simplified period-dependent models for V/H ratios are embedded in some seismic design codes such as National Earthquake Hazards Reduction Program (NEHRP 2009), in order to estimate vertical components from corresponding horizontal spectrum. There are even seismic design codes proposing flat V/H ratios across all periods; for example, the Iran's practical building code (standard no.2800) which recommends a constant value of two-thirds between vertical and horizontal design spectra over all range of periods. Several studies found that clear peak of V/H at short periods exceeds a value of two-thirds in near fault areas (Bozorgnia et al. 1995, 1996; Bozorgnia and Campbell 2004, 2016). Series of studies revealed strong dependency of V/H ratio to spectral period, site effect, and source-to-site distance, while there seems to be less dependency to magnitude and faulting mechanism (Bozorgnia and Campbell 2004). Such degree of dependencies of V/H ratios to site and path characteristics highlights the shortcomings of oversimplified V/H models used in certain design codes. For instance, one of the main deficiencies of such models is the lack of proper consideration of site effect, which in turn undermines the validity of such approaches for site-specific seismic hazard assessments (Bommer et al. 2011). The same applies to path effect (source-to-site distance) which has not been addressed in those simple models. These deficiencies highlight the need for a more rational approach for assessment of V/H ratios, where source, path, and site effects are all taken into account. A direct application of such models is in site-specific seismic hazard assessment as well as modification of seismic design guidelines and codes. Akkar et al. (2014) developed a model for Europe and the Middle East which can be used to estimate V/H ratios for all site conditions,

including soil nonlinearity and as a continuous function of V_{S30} . Development of empirical ground-motion prediction equations (GMPEs) for predicting V/H ratios is a preferred approach which allows direct assessment of V/H ratio as a function of path, site, and source characteristics (Akkar et al. 2014).

Recently, two models were developed by Soghrat and Ziyaeifar (2016b) and Zafarani et al. (2018), hereinafter called SZ16 and Zea18, respectively. The former model was tailored to the Northern Iran only. Both models predict spectral ordinates for periods shorter than 4 s. Both models also account for SoF effects; nevertheless, almost similar predictions were presented for strike-slip and reverse events. Neither Zea18 nor SZ16 include fault rupture in their predictive models.

Soghrat and Ziyaeifar (2016b) examined the applicability of some regional and global V/H ground-motion models (e.g., Gülerce and Abrahamson 2011; Akkar et al. 2014; and Bommer et al. 2011) for Northern Iran and reported weak correlations between recorded Iranian strong motion data and those predicted by the models. Therefore, the present study is an attempt to develop a new V/H ground-motion models based on local strong ground-motion database, recorded across all tectonic regions in Iran. The process in particular pay special attention to the behavior of V/H response spectra at short periods, taking into account that vertical natural periods for most structural components and systems are located at short periods.

Therefore, the proposed V/H ground-motion models predict PGA, PGV, and 5%-damped spectral ratios for a wide range of spectral ordinates from 0.01 to 10 s as functions of moment magnitude, source-to-site distance, style-of-faulting, and ground types. For this purpose, a large well-compiled Iranian ground-motion databank including 1871 three-component records from 420 earthquakes was compiled. The database is considered as an improved and enriched version of the Iranian strong ground-motion database, compared to those used in previous GMPEs for Iran. Extended efforts were invested to enhance the metadata with regard to available style-of-faulting and recording stations with measured V_{S30} which account for 98% (1860 records) and 75% (1399 records) respectively, while for Zea18, the measured V_{S30} values and SoF are available for only 40% and 34% of their dataset, respectively. Moreover, for about 60% of the events used by SZ16, the faulting mechanism is unknown and also only 45% of their selected records are classified

with known V_{S30} . For the remaining records in both studies, V_{S30} values were classified based on empirical methods. This study also uses an updated version of the Iranian strong motion database up to late 2014 which includes additional 38 earthquakes and 140 three-component records happened in 2014, among them 11 events (93 records) with $M_w > 5.0$.

We examined four different functional forms to explore the most appropriate ones for unbiased determination of V/H spectral ratios. All these models predict V/H ratios as functions of source-to-site distance, magnitude, soil conditions, and styles-of-faulting. The compiled database provides various source-to-site distance measures such as R_{epi} (epicentral distance), R_{hyp} (hypocentral distance), R_{JB} (Joyner-Boore distance), and R_{rup} (rupture distance) for each strong motion record. The availability of these distance metrics in our database enabled us to develop consistent V/H models for these distance measures, applicable for distance range of up to 200 km. The examination process includes comparison of median estimates of V/H ratios derived from R_{JB} -, R_{epi} -, R_{rup} -, and R_{hyp} -based models.

Attempts are also made in this paper to examine the validity of the proposed models by studying the aleatory standard deviations and checking residuals, followed by their comparison with some previously published V/H models from local and regional databases.

2 Iranian ground-motion database

The provided Iranian ground-motion database comprised of 1871*3 waveforms from 420 earthquakes recorded at 668 Iranian strong motion stations. All unprocessed acceleration time histories were recorded by Iran Strong Motion Network (ISMN, <http://ismn.bhrc.ac.ir/>), operated, and maintained by the Building and House Research Center (BHRC 2005). Only three-component accelerograms were used in this study. We used direct M_w estimates from the Harvard global CMT catalog (Centroid Moment Tensor 2015), the NEIC global catalog (National Earthquake Information Center 2015), and where necessary (for 130 earthquakes, 289 records out of 1871) converted from M_s and m_b using conversion formulas derived from ISC (International Seismological Centre 2015) catalog, proposed by Shahvar et al. (2013). This database includes earthquakes with $M_w \geq 4.5$ and records with distance ≤ 200 km. Figure 1 shows the geographical distribution of

these earthquakes (indicated by circles) and strong motion stations (shown by black triangles).

The focal mechanism of 251 earthquakes with 1421 records were identified through double-couple fault plane solution using strike, dip and rake angles of fault planes. The remaining 40% of earthquakes (24% of records) could not be associated to any faulting mechanism. Refined investigation was carried out to these data in order to determine the most probable faulting mechanisms through determination of corresponding causative faults. For this purpose, we studied and collected information about seismic characteristics of neighboring active faults (e.g., dip and strike angle) and their corresponding reliable mechanism. Additional information such as style-of-faulting of dependent shocks and their associated active faults, regional tectonic setting, topographic map of vicinity area, and information from previous earthquakes associated to the causative fault are used to assess fault characteristics. In the present study, vast majority of earthquakes (98%) were associated to focal mechanisms. This is a significant improvement compared to the earlier model of Zea18 for which the faulting mechanisms for about 66% of the studied earthquakes were unknown. As is seen in Fig. 2b, the database consists of 187 strike-slip events (811 records) and 217 reverse events (985 records). There were few observations with normal-faulting mechanism (11 out of 420 earthquakes). The M_w - R_{JB} distribution of all records with respect to style-of-faulting is depicted in Fig. 2a. As inferred from this figure, records are well distributed except for $6.7 < M_w < 7.1$ over all distance ranges and for $M_w > 6.5$ and $R_{JB} < 20$ km.

The measured V_{S30} values were available for 433 recording stations (75% of total 1871 records), ranging from 155 to 2400 m/s which shows a notable enhancement compared to the recent model of Zea18, in which 306 stations (40% of their records) had measured V_{S30} . These measurements were made for ISMN through seismic refraction technique by BHRC. In order to have a robust predictive model, records with unknown V_{S30} values (shown as yellow squares in Fig. 1) were removed from the database. Then, the remaining data was classified based on ground type definitions suggested by Iran's building design code as follows: site class I ($V_{S30} > 750$ m/s), site class II ($375 < V_{S30} < 750$ m/s), site class III ($175 < V_{S30} < 375$ m/s), and site class IV ($V_{S30} < 175$ m/s). Only 4 stations with 5 recorded events are included in site class IV which were combined with station with type III classification. As

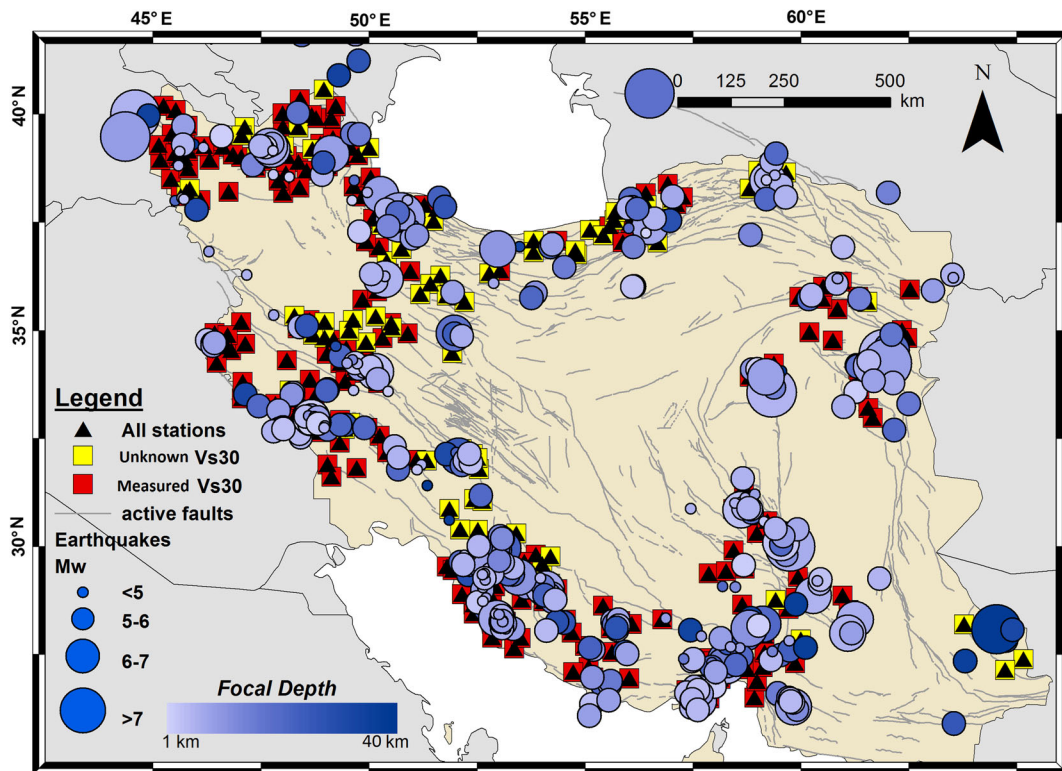


Fig. 1 Geographic distribution of earthquakes and strong ground-motion recording stations across Iran. Stations with unknown V_{S30} (yellow squares) are excluded from the process for V/H model development. Earthquakes are colored by focal depth, as darker

circles represent deeper events and their sizes are proportional to M_w . The gray lines indicate active faults (Zolfaghari and Darzi 2014)

shown in Fig. 3b, 35% of all accelerograms were recorded on site class I, 48% on site class II and 17% on site class III. The M_w – R_{JB} distribution of the selected records grouped in different site classes is shown in Fig. 3a. The scatter plots of records associated to each ground type (I, II and III) show similar distribution for all magnitude–distance intervals.

Focal depth measurements were derived from reliable local and global earthquake catalogs. The local catalog of IRSC (Iranian Seismological Centre, <http://irsc.ut.ac.ir/>) was given higher priority for determining earthquake focal depth. For 3 events with no reliable depth estimates, the Scherbaum et al. (2004) equations were applied to estimate focal depth using

Fig. 2 **a** Magnitude–distance distribution of the compiled database in terms of style-of-faulting. **b** Histogram of number of earthquakes and records versus SoF shown in dark gray and light gray bars, respectively. Reverse faults (RV), SS, and NR stand for reverse, strike-slip, and normal faulting types, respectively

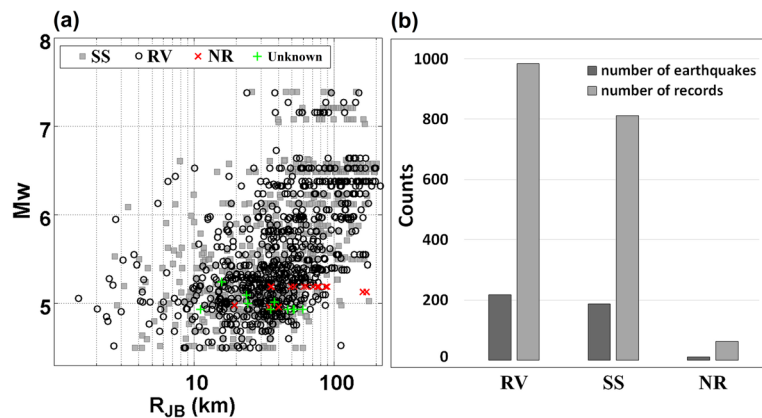
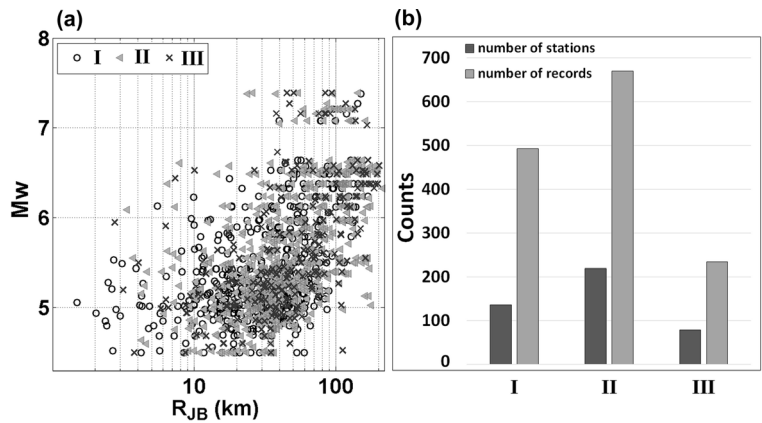


Fig. 3 **a** Magnitude–distance distribution of the compiled database in terms of local site classes. Data points are shown with different symbols for site classes (I, II, and III). **b** Histogram of number of stations and records versus site classes



moment magnitude and style-of-faulting as inputs. In order to avoid unbiased results in terms of earthquake depth, only earthquakes with focal depth less than 40 km (92% of earthquakes) were allowed in the regression analyses. Figure 4 shows the distribution of selected earthquakes with respect to moment magnitude, focal depth, and number of recorded accelerograms *per* earthquake. As can be seen in this figure, a good portion of database is associated with events with multiple records for earthquakes with $M_w > 6$. About 13% of earthquakes are single-recorded events, among which 67% are with $M_w > 5$.

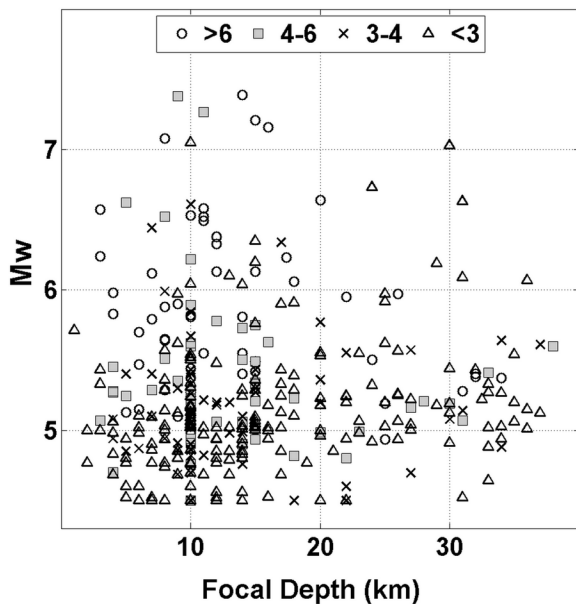


Fig. 4 Magnitude–depth distribution for the selected database. Data points are classified based on number of accelerograms *per* earthquake

In order to make the GMPEs applicable in probabilistic seismic hazard analyses, models based on both finite-fault (R_{rup} and R_{JB}) and point source (R_{epi} and R_{hyp}) distance metrics are presented in this paper. R_{JB} is defined as the horizontal distance to the closest point on the surface projection of the fault rupture (Joyner and Boore 1981), and R_{rup} is the closest distance to fault rupture plane. The R_{JB} , R_{epi} , and R_{hyp} were first computed for all strong motion records in the database. Then, using the procedure described by Kaklamanos et al. (2011), rupture distances (R_{rup}) were estimated for all records in the database. These estimates are made as functions of R_{JB} , dip angle, width of fault rupture plane, depth to top of rupture plane (Z_{TOR}), and source-to-site azimuth.

The final selected database for regression analyses consists of 1350 accelerographic records from 370 earthquakes, recorded during 1975 to 2014. Table 1 shows the proportion of compiled database which was removed to prevent rough records in the regression analyses, such as deep events and recording stations with unknown V_{S30} values.

All waveforms were uniformly corrected for baseline offset based on the approach proposed by Boore et al. (2002) and de-noised using the modified adaptive wavelet de-noising technique proposed by Ansari et al. (2007, 2010). Compared to conventional filtering approaches (e.g., Boore 2005; Boore and Bommer 2005), the applied approach eliminates nonstationary noises in the time domain and attenuates noises for all period range of engineering interest. This facilitates development of a ground-motion model applicable to the broad range of periods, while highly noisy waveforms can be corrected efficiently. Peak ground acceleration (PGA), peak

Table 1 Distribution of data before and after applying filtering criteria for performing regression analyses

	SS	RV	NR	UN SoF	SCI	SCII	SCIII	UN SC	No. of records	No. of events
Initial dataset (%)	43.34	52.65	3.42	0.59	25.2	26.4	35.9	12.5	1871	420
Final dataset (%)	43.73	54	1.34	0.83	35.3	47.7	17	0	1350	370

SC stands for site class. UN stands for unknown. SS, RV, and NR stand for strike–slip, reverse, and normal faulting mechanism, respectively

ground velocity (PGV), and 5%-damped response spectral acceleration (SA), sampled at 60 equally log-spaced vibration periods from 0.01 to 10 s, are included for horizontal and vertical components. The average horizontal ground-motion intensity measures were computed by geometric mean calculation.

3 Functional forms of V/H models

To find the best functional form with optimum performance on the compiled ground-motion database and to avoid shortages caused by complex models, first the distribution of observed V/H ratios w.r.t magnitude and distance is explored. Then, the behavior of median V/H ratios as functions of independent variables and

also the trends of V/H ratios for different scenarios of functional forms are investigated.

Figure 5 shows observed V/H spectral ratios against distance (top row) and magnitude (second row) for PGA and spectral periods of 0.1 and 2 s. Data points are plotted for reverse-faulting events with ground motion recorded on rock site. According to this figure (top row), as distance increases, the V/H ratios tend to decrease at PGA, remain constant at $T=0.1$, and increase at $T=2$ s. The distribution of V/H ratios, however, does not show strong dependency to moment magnitude as shown in the second row of this figure.

The median V/H ratios for PGA and response spectral ordinates of $T=0.1, 2.5,$ and 4 s are shown in Fig. 6. To eliminate the SoF effect, all recording data are initially scaled to reverse faulting through preliminary

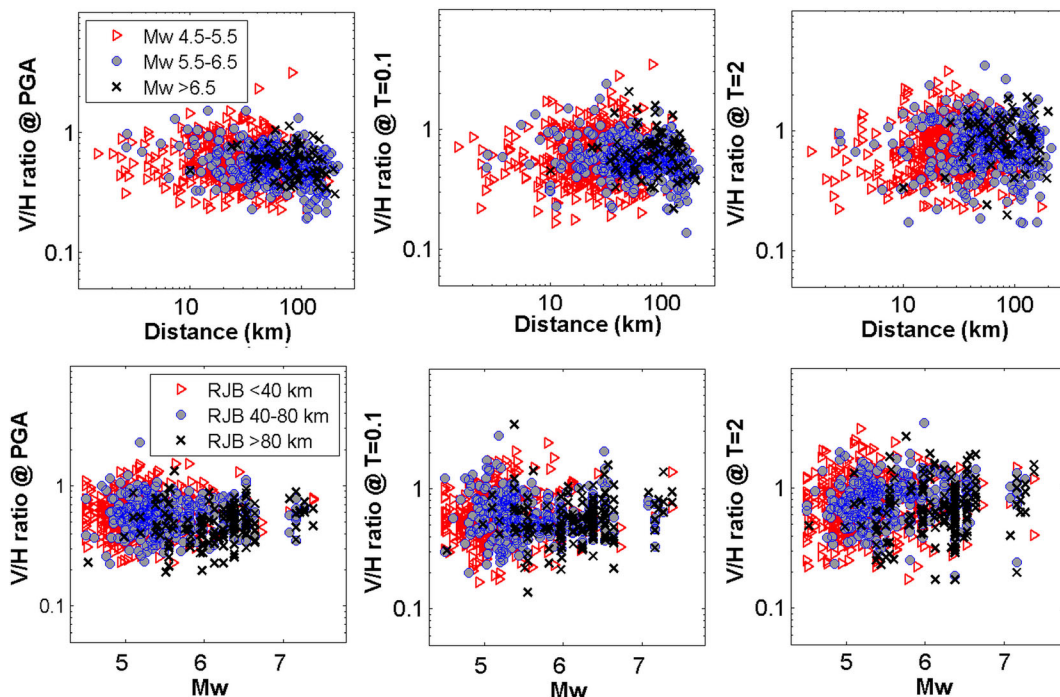


Fig. 5 Distribution of actual V/H spectral ratios against distance (top row) and magnitude (second row) for PGA, $T=0.1$ and 2 s. Reverse faulting events located on rock sites are plotted

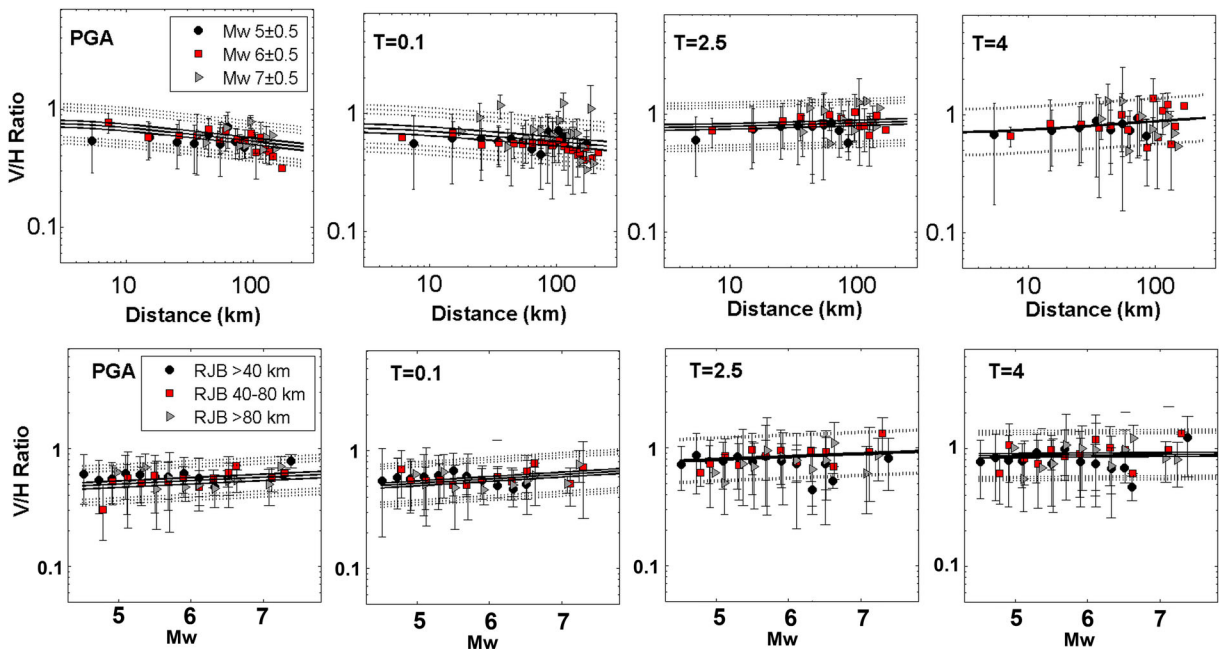


Fig. 6 Median V/H ratios of PGA, $T=0.1$, 2.5, and 4 s as functions of R_{JB} (first row) for three magnitude intervals and M_w (second row) for three distance intervals, for rock sites. Median V/H predictions (black solid lines) and their corresponding standard

deviations (black dotted lines) obtained from the selected functional form are plotted against distance-magnitude cluster which will be discussed in Sect. 4

empirical scaling factors. To explore the effect of distance on the V/H ratios for a given period, data are grouped into three M_w intervals and by 10-km R_{JB} bins as shown in first row of Fig. 6, illustrating median V/H ratio for each distance cluster plotted against corresponding standard deviation. Apparently, the median V/H ratios show decay for PGA with increasing distance, remain independent of R_{JB} for $T=0.1$ s and gradually increase with distance at longer periods. Similar results were also observed in Fig. 5.

In a similar manner, in order to investigate the magnitude dependency of V/H ratios, data are grouped into three R_{JB} intervals and by magnitude bins of 0.1 M_w as illustrated in second row of Fig. 6 which shows cluster of the median V/H ratio for each distance against corresponding standard deviation. As discussed for Fig. 5, magnitude dependency of V/H ratios at different periods is almost negligible for all distance ranges. Similar results were observed by several studies such as Gülerce and Abrahamson (2011), Akkar et al. (2014), and Bommer et al. (2011).

In order to find the most suitable functional form for development of V/H ratio model, four different

functional forms are examined based on the following generic form:

$$\begin{aligned} \log_{10}(V/H) = & b_1 + b_2M_w + b_3M_w^2 + (f_{R1} \text{ or } f_{R2}) \\ & + b_7S_{II} + b_8S_{III} + b_9RV + b_{10}SS \\ & + \varepsilon \end{aligned} \tag{1}$$

where

$$\begin{aligned} f_{R1} = & (b_4 + b_5M_w) \log_{10}(R_1 + b_6); R_1 \\ = & R_{rup} \text{ or } R_{hyp} \end{aligned} \tag{2}$$

$$\begin{aligned} f_{R2} = & (b_4 + b_5M_w) \log_{10}\left(\sqrt{R_2^2 + b_6^2}\right); R_2 \\ = & R_{JB} \text{ or } R_{epi} \end{aligned} \tag{3}$$

The proposed model includes a magnitude scaling term, a geometric decay term as a function of distance, a site amplification variable, and a style-of-faulting factor to estimate median vertical-to-horizontal ground-motion ratio (denoted as V/H in Eq. 1) which can be either PGV, PGA, or 5%-damped response SA at

periods from 0.01 to 10 s. The $b_3M_w^2$ term accounts for magnitude saturation effects. The geometric attenuation term of f_{R1} in Eq. (2) is considered for R_{rup} or R_{hyp} distance metrics, and the term f_{R2} in Eq. (3) is with respect to R_{JB} or R_{epi} distance metric. Contrary to our model, Akkar et al. (2014) used similar functional form for three R_{JB} -, R_{epi} -, and R_{hyp} -based GMPEs for Europe and the Middle East. The b_5M_w term takes into account magnitude-dependent geometrical spreading. Note that in case of small events ($M_w < 5$), R_{rup} and R_{JB} are almost equal to R_{hyp} and R_{epi} , respectively.

RV and SS are dummy variables taking the value of 1 for reverse and strike–slip faulting mechanism, respectively, and 0 for unknown SoF. S_{II} and S_{III} are also dummy variables accounting for site categories defined by Iran’s building design code based on V_{S30} values, where $S_{II} = S_{III} = 0$ represents site class I (rock site, $V_{S30} > 750$ m/s); $S_{II} = 1$ and $S_{III} = 0$ are for site class II ($375 < V_{S30} < 750$ m/s); and $S_{III} = 1$ and $S_{II} = 0$ are for site class III ($V_{S30} < 375$ m/s). In Eq. (1), ε represents the error term which is normally distributed in logarithmic units with standard deviation of sigma ($\sigma_{(\log_{10} V/H)}$). The total sigma decomposed of between-event (τ , inter-event) and within-event (φ , intra-event) aleatory standard deviations resulting from the regression procedure, as given by the following expression:

$$\sigma_{(\log_{10} V/H)} = \sqrt{\tau_{V/H}^2 + \varphi_{V/H}^2} \quad (4)$$

Based on the generic form shown in Eq. (1), four different scenarios of functional forms were investigated in this study. Functional form (1) excludes the magnitude-dependent geometric spreading coefficient ($b_5 = 0$). Functional form (2) ignores the magnitude-dependent saturation coefficient ($b_3 = 0$). Functional form (3) simplifies the base equation by removing both b_5 and b_3 coefficients ($b_5 = b_3 = 0$). Functional form (4) includes anelastic attenuation effect (mostly at long-distances $R > 80$ km) by adding ($+b_{11}R$) term. We constrained $b_6 = 5$ km while evaluating the functional forms and obtained other coefficients by conducting nonlinear least-square regression analyses to each functional form. Note that due to insignificant effect of SoF pointed out by SZ16 and Zea18, we did not consider such dependency.

Figure 7 compares the median V/H trends as a function of R_{JB} for M_w 5, 6 and 7. Comparisons are made for PGA and spectral periods of 0.5 and 3 s along with V/H ratio observations for M_w 5 ± 0.2 , 6 ± 0.2 , and 7 ± 0.2 for

site class II. Each row in Fig. 7 represents the median V/H estimates derived from one of the four functional forms described earlier. Figure 7a, b, c, and d are associated to functional forms (1), (2), (3), and (4), respectively.

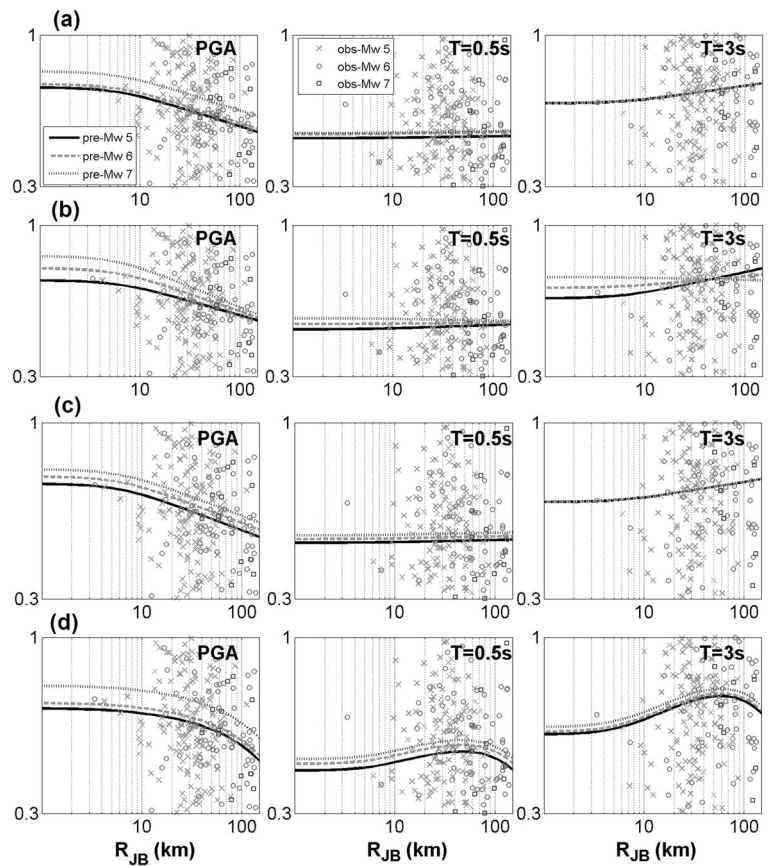
As shown in Figs. 5 and 6 and also pointed out by other researchers (e.g., Bommer et al. 2011; Gülerce and Abrahamson 2011), the V/H ratios tend to attenuate faster at very short periods and flatten and increase gradually towards longer periods. Detailed investigation on the reasons for such pattern is given by Gülerce and Abrahamson (2011), and the seismological explanations are offered by Beresnev et al. (2002) and Kawase and Aki (1990).

Functional form (1), including a quadratic dependence on M_w (Fig. 7a), shows similar trends as noted above. At very short periods, the V/H ratios tend to mildly attenuate with increasing distance; at $T = 0.5$ s, they are constant; and for $T > 0.5$ s, they rise smoothly with distance. Although for PGA and for events with M_w 5 and M_w 6, median curves are closer to each other; their overall behavior is quite reasonable and consistent with the actual data trends. At long periods, the median V/H ratios for events with M_w 7 overlap the corresponding V/H ratios of M_w 6 and M_w 5. Soghrat and Ziyaeifar (2016b) observed stronger magnitude dependency for data from Northern Iran than those pointed out by Bommer et al. (2011) for Europe and the Middle East; however, they could not find a meaningful trend and decided to discard b_3 and b_5 coefficients.

For functional form (2) (Fig. 7b) and for PGA and $T = 0.5$ s at $R_{JB} > 20$ km, V/H curves corresponding to different magnitude levels tend to converge. Moreover, at long period ($T > 0.5$ s), the median V/H ratios for curves representing to M_w 5 overlap with those for M_w 6 and subsequently M_w 6 median curves overlap the M_w 7 median curve at $R_{JB} > 40$ km. These trends are contrary to the actual data pattern. The results of functional form (3) (Fig. 7c), which is the simplest applied model, are similar to the first functional model, and they are both in good agreement with the V/H ratios of actual data.

As shown in Fig. 7d, the predicted median V/H ratios based on functional form (4) reveal an unreasonable behavior with decreasing trend at long distances. Thus, it is revealed that applied database in this study does not allow to capture magnitude-dependent geometric spreading term, neither additional anelastic attenuation term.

Fig. 7 Median V/H ratios trends against R_{JB} for PGA and spectral periods 0.5 and 3 s as functions of M_w (5, 6, and 7) obtained from four alternative functional forms. **a** Functional form (1). **b** Functional form (2). **c** Functional form (3). **d** Functional form (4). V/H observations from site class II are plotted for M_w 5 ± 0.2 , 6 ± 0.2 , and 7 ± 0.2



Comparing the stability and significance of the coefficients of the models derived from different functional forms, the coefficients associated to functional form (3) showed better stability and smoothness over the whole range of periods, while other models presented unpleasant and undesirable jaggedness for b_1 , b_2 , and b_3 , especially for $T > 0.7$ s. Besides, b_4 , as an important coefficient representing attenuation with distance, was completely unstable in functional form (2). Furthermore, we evaluated the residuals of different functional forms and found that functional forms (1) and (3) represent more unbiased models compared to functional forms (2) and (4). Altogether, we believe that functional forms (1) and (3) show better stability in the multi-step maximum-likelihood regressions procedure and, therefore, represent the most reasonable fits among four alternative forms. In conclusion, authors decided to examine performance of both functional forms through further investigations using standard deviations and residual analyses.

4 Regression analyses

In this section, two-stage maximum-likelihood regression technique (Joyner and Boore 1993, 1994) was performed to compute the period-dependent coefficients and aleatory variability for selected functional forms. This technique was applied to functional forms (1) and (3) for four scenarios associated to different distance metrics as discussed earlier. In the first step, the regression analyses were undertaken on all data and site amplification coefficients (b_9 and b_{10}) and b_4 . Through this process, the within-event aleatory (φ) variability's were determined from the first stage of regression, while magnitude scaling coefficients (b_1 , b_2 , and b_3) and between-event variability (τ) were derived from the second stage. For detailed explanation on regression procedure, please refer to Darzi et al. (2018). Note that site class I is considered as reference rock ground type. In final step, by fixing b_1 and b_2 (and b_3 for functional form (1)) to the values derived from the previous step, the regression analyses were repeated to estimate the

coefficients for focal mechanism predictors. In this way, predicted ground-motion intensities were scaled with regard to magnitudes to become equal for different faulting mechanisms (following Cauzzi and Faccioli 2008). In this step, regression analyses were performed to earthquakes with more than 3 ground-motion records with $5 < M_w < 6$, which constitutes the majority of accelerograms with almost the same number of reverse and strike–slip events. This leads to reduction of between-event uncertainty component of the predictive model by average 20% over all vibration periods and up to 40% at some long periods. It should be noted that due to the small number of normal and unknown faulting earthquakes (29 records), they have been removed from this regression step. Another point to note is that all coefficients are period-dependent, except b_6 (saturation term of fictitious depth, in Eqs. (2) and (3)), which is kept constant at 5 km.

Some recently developed V/H models (Akkar et al. 2014; Gülerce and Abrahamson 2011) considered nonlinear site effect, whereas Bommer et al. (2011) and Zea18 did not account for nonlinear site term. The nonlinear site effects, which mostly influenced the horizontal components of ground motions, have not been implemented in our models. This is due to the deficiency of our dataset with regard to factors controlling nonlinearity such as strong intensity measures at very short distances and at stations located on soft soil. Zea18 and Sedaghati and Pezeshk (2017) too neglected nonlinear site amplification effect in their recent GMPEs developed for horizontal component in Iran due to the same reasons as well as weak influence of soil nonlinearity in their dataset.

It should be highlighted that the V/H prediction models accounting for nonlinear site response can only be applied to the horizontal-GMPEs including nonlinear effects. Therefore, as mentioned earlier, due to lack of such horizontal ground-motion models for Iran, development of V/H model based on nonlinear site-response would not be applicable at the present time. Moreover, it is a common practice to explore nonlinear site response analysis as part of site specific PSHA studies. Nevertheless, the significance of soil nonlinearity in Iranian ground-motion database deserved to be studied in more detail, taking into account the seismicity of the country as well as relatively dense strong motion network in Iran.

The coefficients derived from regression analyses for the proposed V/H models and their corresponding uncertainty components for PGV, PGA, and 5%-damped

response spectral acceleration from 0.01 to 10 s are all available as Electronic Supplement A to this paper. Table 2 lists the period-dependent coefficients, the intra- and inter-event uncertainty components, and total uncertainty for R_{JB} -based model derived from functional form (1) for some selected vibration periods.

Similar processes were taken for the functional form (3). For the sake of brevity and not to crowd the figures, hereinafter, all plots and results are shown for functional form (3), while only the results derived from functional form (1) are reported. Moreover, the V/H ground-motion models for R_{rup} , R_{hyp} , R_{JB} , and R_{cpi} are developed following similar steps, except utilizing different geometric attenuation terms described in Sect. 3.

In Fig. 8, median V/H ratios and their corresponding standard deviations are compared against observed V/H ratios as a function of distance classified by M_w 5 ± 0.2 , 6 ± 0.2 , and 7 ± 0.2 in the top row, as well as w.r.t moment magnitude classified by R_{JB} 30 ± 10 , 60 ± 20 , and 110 ± 30 km. Comparisons are made for PGA and spectral acceleration at $T = 0.1$, 1, and 3.5 s. As it can be seen, the proposed model agrees fairly well with the original V/H data. Similar results were also found for other site classes.

Moreover, in Fig. 6, the predicted median V/H (black solid lines) for rock sites and their corresponding standard deviations (black dotted lines) obtained from functional form (3) are depicted for M_w 5, 6, and 7 in the top row and for R_{JB} 30, 60, and 110 km, in the bottom row. Apparent from the figure, there is not much difference between the predicted and observed median V/H at different periods.

In Fig. 9, we compared period-dependent variations of within-event (φ), between-event (τ), and total (σ) standard deviations of the proposed model in this study based on functional form (3) with four local and regional models. These comparative V/H models are SZ16 for Northern Iran; Zea18 for all Iranian territory; Akkar et al. (2014), hereinafter ASA14; and Bommer et al. (2011), hereinafter BAK11 for Europe and the Middle East.

In our model, τ ranges from 0.038 to 0.1 and has small contribution in total sigma, while φ ranges from 0.124 to 0.207 and is a major contributor to the total sigma values of our model. Also, total sigma tends to increase as shifting towards longer periods from 0.137 to maximum value of 0.216 at $T = 8$ s. The ranges of total sigma dependency to spectral periods for various V/H models are as follows: from 0.16 to 0.2 for ASA14, from 0.163 to 0.21 for BAK11, from 0.21 to 0.27 for SZ16, and from

Table 2 Regression coefficients for the functional form (1) based on R_{JB}

T (s)	b_1	b_2	b_3	b_4	b_6	b_7	b_8	b_9	b_{10}	φ	τ	σ
PGV	0.226	-0.064	0.010	-0.182	5	0.010	-0.015	-0.023	0.025	0.136	0.084	0.160
PGA	0.301	-0.145	0.015	-0.121	5	-0.024	-0.066	-0.012	0.013	0.126	0.056	0.138
0.01	0.301	-0.145	0.015	-0.121	5	-0.024	-0.066	-0.012	0.013	0.126	0.056	0.138
0.02	0.268	-0.121	0.013	-0.138	5	-0.026	-0.066	-0.012	0.013	0.125	0.056	0.136
0.03	0.437	-0.139	0.015	-0.197	5	-0.030	-0.070	-0.015	0.016	0.127	0.064	0.142
0.04	0.498	-0.138	0.015	-0.228	5	-0.034	-0.078	-0.020	0.022	0.130	0.074	0.150
0.05	0.350	-0.084	0.011	-0.239	5	-0.019	-0.062	-0.014	0.016	0.134	0.080	0.156
0.06	0.167	-0.034	0.007	-0.217	5	-0.001	-0.035	-0.013	0.014	0.137	0.080	0.159
0.07	0.194	-0.059	0.009	-0.185	5	0.012	-0.034	-0.017	0.018	0.138	0.088	0.164
0.08	0.713	-0.255	0.025	-0.157	5	0.028	-0.006	-0.021	0.022	0.143	0.077	0.163
0.1	0.629	-0.276	0.027	-0.091	5	0.033	-0.003	-0.014	0.015	0.151	0.064	0.164
0.2	0.211	-0.178	0.017	-0.035	5	-0.024	-0.075	-0.002	0.002	0.158	0.066	0.171
0.3	0.431	-0.259	0.023	0.019	5	-0.089	-0.155	0.006	-0.006	0.159	0.055	0.168
0.4	-0.702	0.153	-0.012	-0.008	5	-0.106	-0.167	0.004	-0.005	0.159	0.059	0.169
0.5	-0.907	0.231	-0.020	0.017	5	-0.109	-0.170	0.002	-0.002	0.160	0.068	0.174
0.75	-0.854	0.206	-0.018	0.050	5	-0.103	-0.152	0.001	-0.001	0.171	0.070	0.185
1	-0.514	0.096	-0.009	0.028	5	-0.085	-0.131	0.010	-0.010	0.170	0.086	0.190
1.5	-0.411	0.059	-0.005	0.034	5	-0.086	-0.144	0.017	-0.018	0.167	0.088	0.188
2	-1.131	0.305	-0.024	0.020	5	-0.066	-0.134	0.029	-0.031	0.166	0.084	0.186
2.5	-1.092	0.293	-0.023	0.031	5	-0.073	-0.117	0.027	-0.029	0.165	0.075	0.181
3	-0.966	0.241	-0.020	0.063	5	-0.064	-0.101	0.030	-0.033	0.165	0.094	0.190
3.5	-0.887	0.209	-0.017	0.076	5	-0.060	-0.119	0.031	-0.033	0.173	0.104	0.201
4	-0.827	0.197	-0.017	0.074	5	-0.057	-0.102	0.030	-0.033	0.175	0.106	0.205
5	-0.874	0.210	-0.018	0.085	5	-0.055	-0.076	0.035	-0.038	0.186	0.096	0.209
6	-0.818	0.190	-0.016	0.066	5	-0.050	-0.075	0.034	-0.037	0.190	0.092	0.211
7	-1.081	0.286	-0.024	0.056	5	-0.051	-0.082	0.035	-0.039	0.202	0.072	0.215
8	-1.007	0.259	-0.022	0.056	5	-0.049	-0.083	0.037	-0.042	0.207	0.063	0.216
9	-1.092	0.282	-0.024	0.064	5	-0.059	-0.092	0.035	-0.040	0.207	0.055	0.214
10	-1.084	0.270	-0.022	0.067	5	-0.062	-0.094	0.031	-0.036	0.199	0.053	0.206

T stands for period

0.18 to 0.23 for Zea18. Immediately apparent from this comparison is that the aleatory variability of our presented model yields the lowest values over the whole period ranges.

Compared to both local models of SZ16 and Zea18, the within-event standard deviation of our model is significantly lower, while the between-event variability is similar to others. This is due to application of a more comprehensive and reliable metadata and quite uniform distribution of data in terms of distance, especially R_{JB} and R_{rup} . We should highlight that specifically larger number of records with known ground types is provided in this study and more importantly only records with

measured V_{S30} values are used in the regression analyses. This had a significant role in reduction of within-event variability of our model. Unlike present study, both SZ16 and Zea18 models used empirical methods to assign site classes for a large portion of records with unknown site classes. Compared to regional and global models, the observed discrepancies may also stem from the database differences, different distance metrics, metadata completion, and insufficient small magnitude events.

It should be noted that there are minor discrepancies between the standard deviations calculated from functional forms (1) and (3). Moreover, due to imperceptible

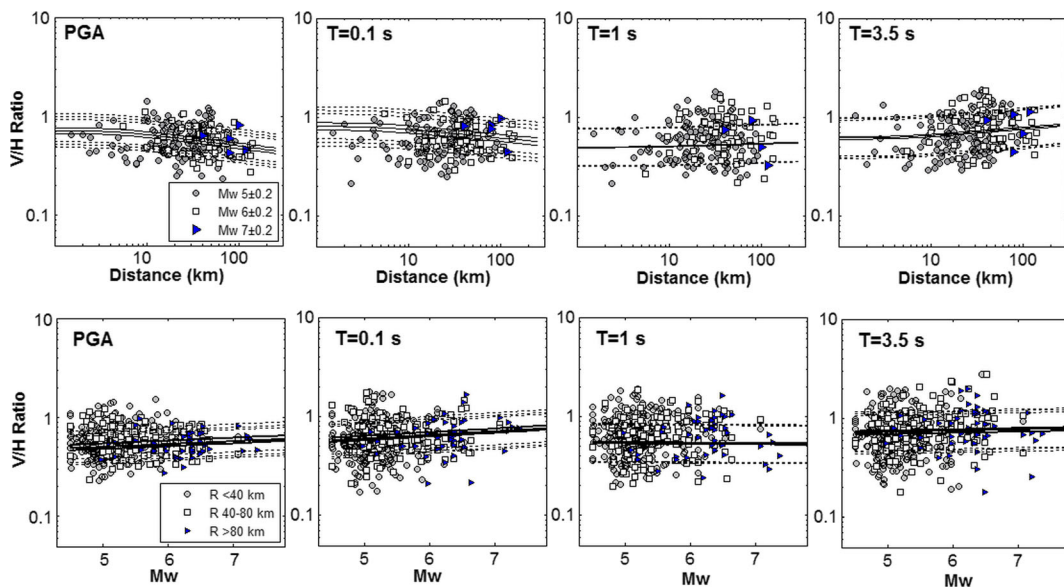


Fig. 8 Comparison between observed V/H and predicted median V/H (solid black lines) and their standard deviations (black dashed lines) for rock sites and events of M_w 5, 6, and 7 (first row) and R_{JB} 30 ± 10 , 60 ± 20 , and 110 ± 30 km (second row)

discrepancies among the total sigma of four considered distance measures, their corresponding curves overlap each other completely. Thus, we decided not to plot them herein. Derived values are tabulated as Electronic Supplement A to this paper.

5 Attenuation of V/H ratios w.r.t various distance measures

In Fig. 10, we explore the differences between the V/H spectral ratios predicted from four individual V/H

ground-motion models developed based on distance metrics of R_{JB} , R_{epi} , R_{hyp} , and R_{rup} using similar ground-motion database.

Figure 10 b compares the variation of median V/H ratios against periods for various source-to-site measures at 20 km. The predictions are for site class II and reverse earthquakes with M_w 6. As shown here, the largest discrepancies between the V/H ratios corresponding to different distance metrics are immediately apparent at short periods ($T < 0.1$ s) and $2.5 < T < 6$ s. Otherwise, there is negligible differences between different models. Akkar et al. (2014) found similar patterns

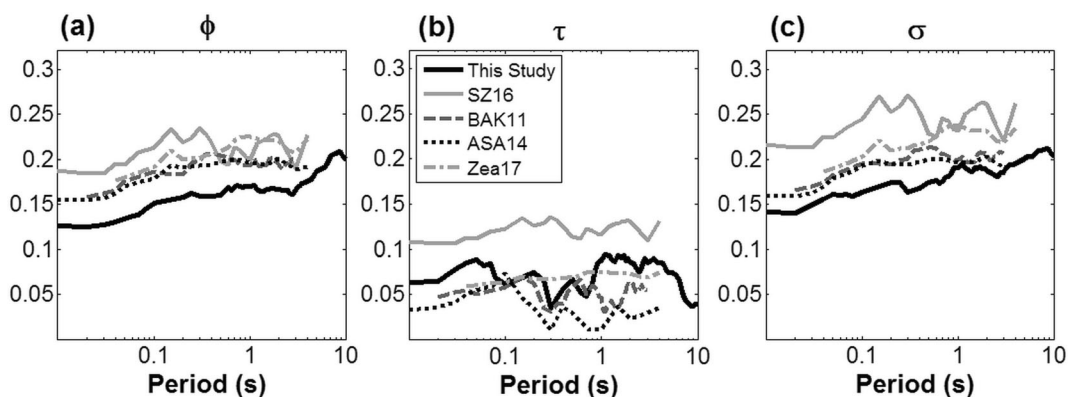


Fig. 9 Comparison of the **a** within-event (ϕ), **b** between-event (τ), and **c** the total (σ) standard deviation for GMPEs proposed in this study based on functional form (3) (thick black lines) with SZ16

(Soghrat and Ziyaeifar 2016b), ASA14 (Akkar et al. 2014), BAK11 (Bommer et al. 2011), and Zea18 (Zafarani et al. 2018)

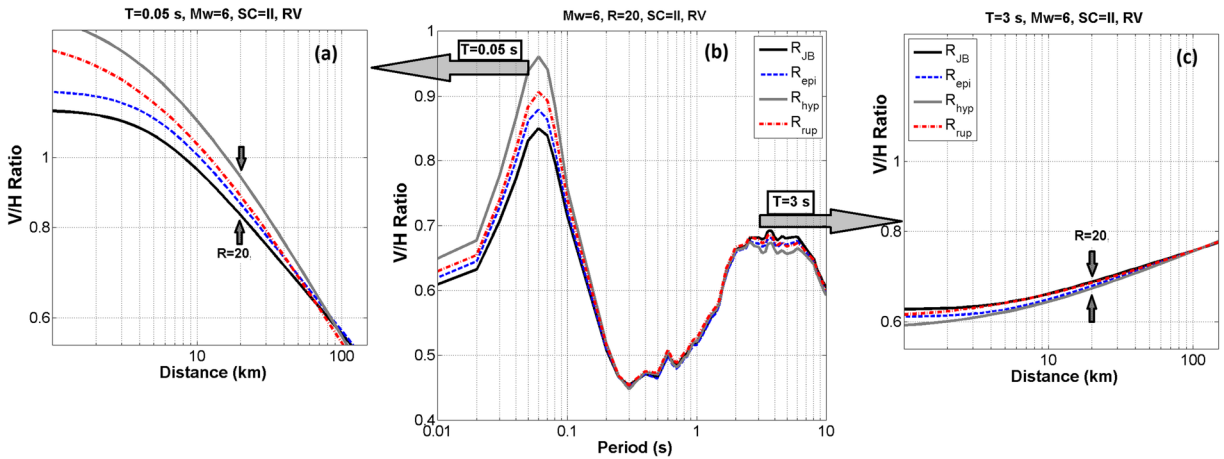


Fig. 10 Comparison of median V/H estimated from models developed based on R_{JB} , R_{epi} , R_{hyp} , and R_{rup} ; as a function of period for $R=20$ km (b), and as a function of distance, at $T=0.05$ s (a) and

$T=3$ s (c). V/H ratios are estimated for site class (SC) II, reverse faults (RV) and for $M_w=6$. All models derived from the same database

towards large magnitudes with less than 5% discrepancies between median V/H values estimated from R_{JB} , R_{epi} , and R_{hyp} -based models for Europe and the Middle East. In Fig. 10, as magnitude increases, the differences between the plotted models increase as well. This is probably due to effect of large rupture dimensions on seismic energy propagation, especially for large earthquakes.

Figure 10a and c show the trend of median V/H ratios against distance for periods at 0.05 and 3 s, respectively. As illustrated in these figures, the curves converge as distances increase, so that for distances greater than 60 km, the V/H predictions are not sensitive to distance metrics which is due to reduction in the effect of focal depth and rupture dimensions. Comparing Fig. 10a–c, it is apparent that at short periods the R_{hyp} -based model predicts the highest V/H ratios and the R_{JB} -based model estimates the lowest values, whereas, at $T=3$ s, the results reversed.

6 Validation of V/H models

In this section, conventional residual analysis was carried out to evaluate the validity of the proposed V/H models. The V/H predictions made in this section are all calculated from the R_{JB} -based model. Residual of V/H spectral ratio, denoted as $res(T)_i$ in the following equation, is calculated from the observed ground-motion amplitudes of V/H spectral ratios (denoted as $obs(T)_i$) with respect to its corresponding

predictions derived from proposed model (denoted as $pre(T)_i$), as follows:

$$res(T)_i = \log_{10}(obs(T)_i) - \log_{10}(pre(T)_i) \quad (5)$$

Residuals are decomposed to between- and within-event residuals which are assumed to have a normal distribution with zero mean and standard deviation of τ and φ , respectively, as presented in Eq. (4).

Figure 11 shows the between-event residuals against M_w for PGA, PGV, and spectral periods of $T=0.1, 0.5, 1,$ and 5 s. Note that positive and negative residuals represent underestimation and overestimation of our proposed model respectively. The two black solid lines in each panel represent the $\pm 1\sigma$ bounds around the medians. The black squares indicate average values of residuals computed at different magnitude bins. Clustering of black squares close to zero reveals unbiased prediction of the V/H values in terms of their corresponding estimator parameters. According to the results indicated in Fig. 11, there is not any model misfit in terms of M_w . Only slight dispersive behavior of residuals is apparent for large magnitudes at all periods which is most likely due to poor distribution of data. To better visualize the possible trends in terms of depth, residual points are classified by earthquake depth as indicated in legend. This figure does not show any apparent trends for deeper events.

Figure 12 shows the within-event residuals plotted as a function of R_{JB} for PGA, PGV, and spectral ordinates of 0.1, 0.5, 1, and 5 s. The residuals do not show any apparent distance dependency, especially for $R_{JB} <$

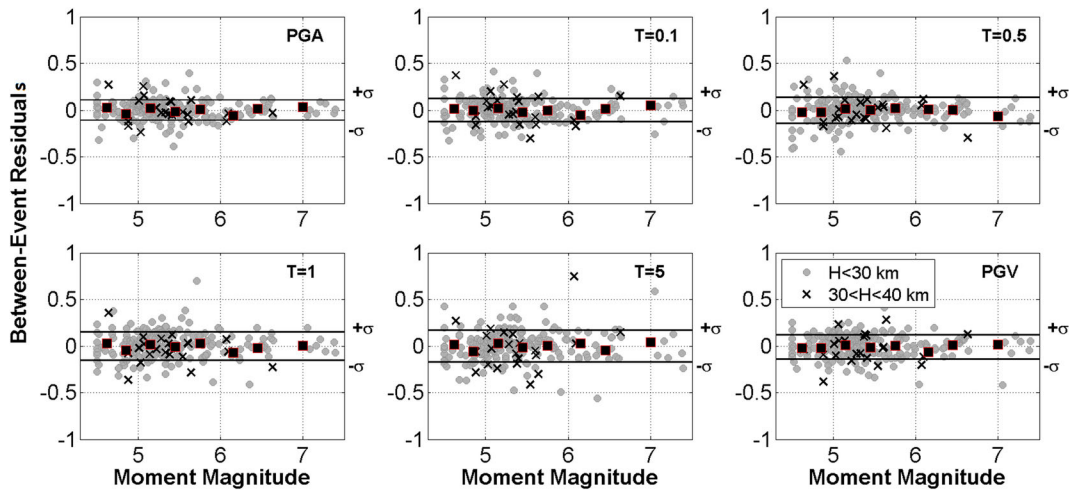


Fig. 11 Between-event residuals as a function of M_w , determined using the proposed R_{JB} -based V/H model, shown for PGA, four spectral periods ($T = 0.1, 0.5, 1,$ and 5 s), and PGV. Residual points

are classified according to the focal depth. Two horizontal lines in each panel represent $\pm 1\sigma$ bounds of the predictions. Black squares represent mean residuals at magnitude bins

150 km, as the average residual values attain a zero value. Despite poor distribution of data at short distances ($R_{JB} < 10$ km), their corresponding mean values of residuals are zero indicating unbiased trend. Moreover, residuals are classified in three site classes (i.e., I, II, and III) to explore any observable trend. The uniform distribution of residuals within $\pm 1\sigma$ bounds confirms an acceptable level of reliability in the V/H estimated from the site terms of the proposed model. In general, the overall behavior of all residuals over the whole period is satisfactory.

Figure 12 was plotted with respect to three other models of R_{rup} , R_{hyp} , and R_{epi} , and similar results were

observed. For the sake of brevity, they are not reproduced here.

The within-event residuals as a function of V_{S30} are presented for PGA and $T = 0.2$ and 3 s in Fig. 13. Residuals are classified by site classes as indicated in the legend. As illustrated, despite clustering of residual points at long periods, the overall observations do not show any systematic trends, suggesting a good performance in the predicted median V/H computed from the developed model. Furthermore, residuals tend to scatter slightly for $V_{S30} > 900$ m/s especially at long periods which may be the results of sparse data. However, the

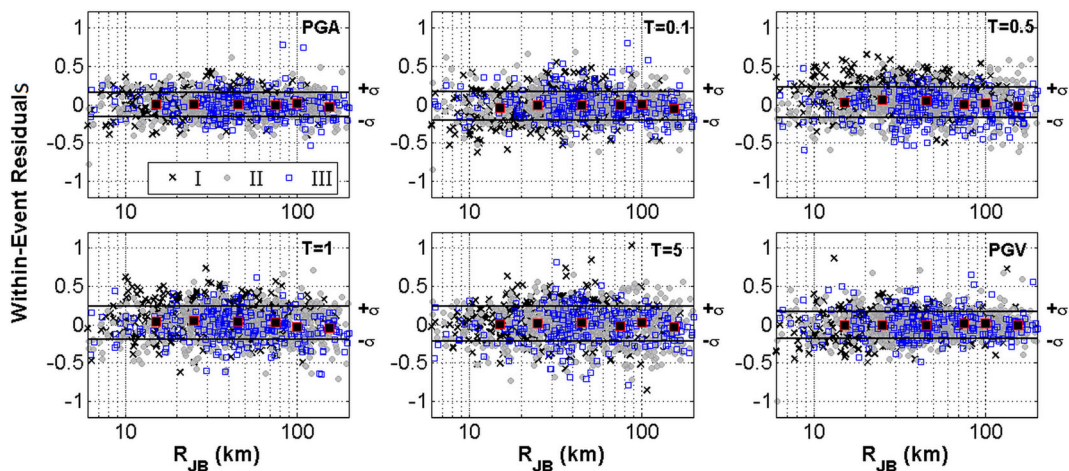


Fig. 12 Within-event residuals as a function of R_{JB} , determined using the proposed R_{JB} -based V/H model, shown for PGA, four spectral periods ($T = 0.1, 0.5, 1,$ and 5 s) and PGV. Residuals are

classified according to the site classes. Two horizontal solid lines represent $\pm 1\sigma$ bounds of the predictions. Black squares represent mean residuals at distance bins

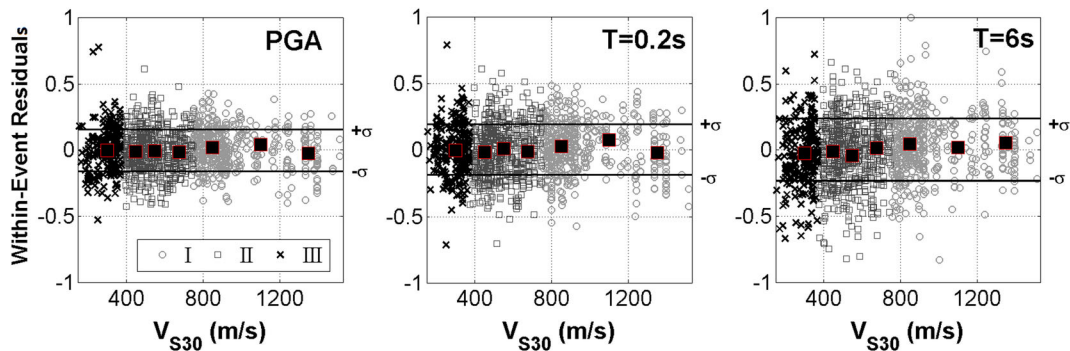


Fig. 13 Within-event residuals of V/H value as a function of V_{S30} and site classes (I, II, and III), shown for PGA, $T=0.2$ and 6 s. Two horizontal solid lines represent $\pm 1\sigma$ bounds of the predictions. Black squares represent mean residuals at V_{S30} bins

variation of residuals is weak and can be neglected. As apparent from residuals distribution depicted in Fig. 13, the variation of V/H data shows no biased trend which could imply independency of the model to nonlinear soil behavior as also shown by Zea18.

As expected, the residuals suggest that V/H models presented in this study are well calibrated so that the assumed V/H models are in good agreement with the observed data in Iran. It should be noted that all residuals are plotted for V/H predictions of functional form (1), and similar results have been captured for functional form (3) as well. Due to negligible differences of two equations, results are not plotted in this paper.

7 Evaluation of predicted V/H spectral ratios

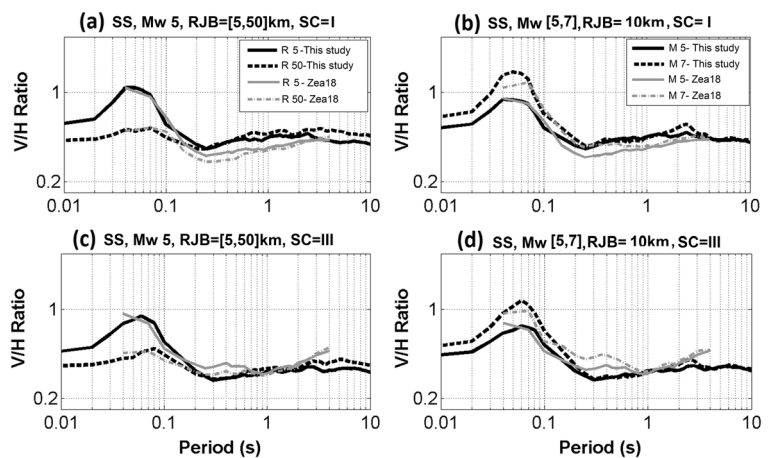
In this section, the effect of explanatory model predictors (i.e., site classes, M_w , R_{JB} , and SoF) is explored under different scenarios. Furthermore, detailed

comparisons are made between the predicted V/H ratios made by this study against a recently published model of Zea18. Similar definition of average horizontal component is used for both models.

Figure 14 illustrates the median V/H over the entire periods for the specific combinations of M_w and R_{JB} . The V/H ratios are evaluated for rock site condition (class I or $V_{S30} = 800$ m/s, if required) and soft soils (class III or $V_{S30} = 400$ m/s, if required) which are shown in top and bottom rows, respectively. To investigate the impact of R_{JB} and M_w , the V/H spectral ratios are plotted for R_{JB} [5, 50] km and for M_w 5 in the left panels and for M_w (Bindi et al. 2010; Boore 2005) and R_{JB} 10 km in the right panels along with their comparison with Zea18 indicated as gray curves. All models are for strike–slip faulting.

The V/H ratios show the highest value at short periods (0.04 to 0.08 s) and the lowest value at periods of 0.2 to 0.35 s (Fig. 14). As inferred from Fig. 14a and c, the peaks increase slightly as distance increases (~ 0.05

Fig. 14 The median V/H ratios obtained from proposed R_{JB} -based model (black lines) compared against those from Zea18; for site class I (top rows) and site class III (second rows), and for M_w 5 and R_{JB} [5, 50] km (left panels), and for M_w (Bindi et al. 2010; Boore 2005) and R_{JB} 10 km (right panels). SS stands for strike–slip faulting



to 0.08 s). Similar to finding by Zea18, V/H estimations show higher dependency to R_{JB} than to M_w . However, V/H dependency to M_w for our model is not as weak as SZ16 model for Northern Iran. As indicated, at $0.3 < T < 2.5$ s, V/H estimates increase smoothly with increasing period similar to BAK11 model for Europe and the Middle East and also the global model proposed by Bozorgnia and Campbell (2004), while for longer periods, they decrease gradually, similar to the Bozorgnia and Campbell (2016) global model. At long distances, larger V/H estimates are apparent which is most probably caused by small magnitude events. Zea18 (gray curves) estimates approximately similar V/H ratios, except for $T > 0.15$ s, on rock site whose predictions are lower than ours.

Peak amplitude of V/H spectral curve at short period exceeds 1.0 at near-source fields (black solid curve in Fig. 14a) and large magnitude events (black dashed curve in Fig. 14b), as similarly observed by several other researches (e.g., Bommer et al. 2011; Bozorgnia and Campbell 2004, 2016). This is thoroughly contrary to Iran's practical building design code which considers constant ratio of two-thirds for all periods. This value is lower on soil sites (Fig. 14d) than rock sites (Fig. 14b).

Figure 15a compares the median V/H spectral predictions for different SoF (Fig. 15a) and ground types (I, II, and III) (Fig. 15b) for M_w 5. The modeled site is located at R_{JB} of 10 km. According to Fig. 15a, the predicted median V/H ratios resulting from strike-slip earthquakes are dominant at short-period ranges ($T < 0.2$ s), while estimations obtained from reverse-thrust events increase smoothly when moving towards longer periods, consistent with SoF pattern appeared in predictive V/H models of Gülerce and Abrahamson (2011) and BAK11. Compared to our model, Zea18 predicts almost equal V/H

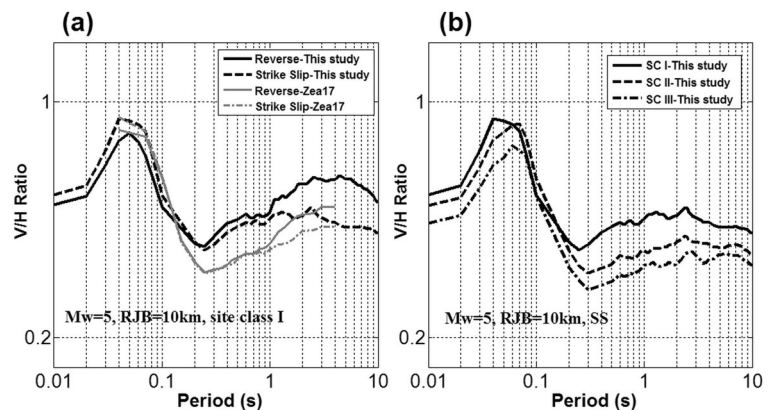
ratios for $T < 0.7$ s with no differences for different SoF and for longer periods predicts lower amplitudes.

The immediate observation from the comparative plots of Fig. 15b is that our predictions are the largest for rock ground types for almost all periods, except for $0.06 < T < 0.2$ s. Note that if soil nonlinearity were considered in our model, we would have expected larger V/H predictions at short spectral periods for large magnitudes at soil sites and short source-to-site distances. Notwithstanding minor discrepancies of the median V/H predictions at short periods, site term influence becomes apparent at intermediate-to-long periods for Iranian database, similar to what was observed by Zea18 and BAK11. Unlike our model, Bozorgnia and Campbell (2016) found significant differences for different V_{S30} values (see Fig. 9) in NGA-West2 dataset, especially at short periods. At longer periods, as sites are representing softer layers, they are expected to have a lower V/H which. This trend is consistent with SZ16 and BAK11 models which are developed for Northern Iran and Europe and the Middle East, respectively.

8 Comparison with other studies

Figure 16 presents the comparison between the predicted median V/H spectral ratios made by this study with two recently published local models of SZ16 and Zea18 for Iran as well as two regional V/H models of BAK11 and ASA14 for Europe and the Middle East. Comparisons are made reverse-faulting events of M_w 5 (first column) and M_w 7 (second column) and for R_{JB} 10 km (first row) and R_{JB} 50 km (second row). Note that vertical axis has similar scale for all panels.

Fig. 15 Median V/H ratios obtained from proposed R_{JB} -based model. **a** Reverse and strike-slip faulting mechanism compared with the results of Zea18. **b** For site class I (solid lines), II (dashed lines), and III (dot-dashed lines); for M_w 5 and R_{JB} 10 km



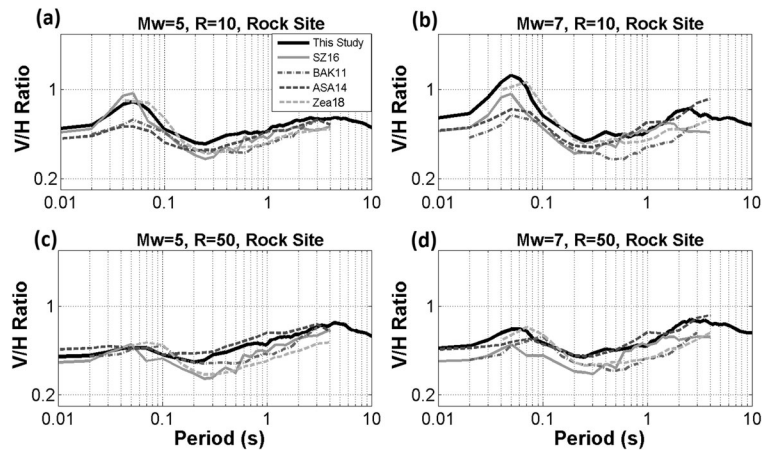


Fig. 16 Comparison of predicted median V/H by this study (solid black lines) with those predicted by selected V/H models of SZ16 (Soghrat and Ziyaeifar 2016b), BAK11 (Bommer et al. 2011), ASA14 (Akkar et al. 2014), and Zea18 (Zafarani et al. 2018) for

rock site (class I, $V_{S30} = 800$ m/s, if needed). The plots are for reverse events with M_w 5 (left panels) and 7 (right panels), at R_{JB} 10 km (first row) and 50 km (second row)

In terms of site term definition, all comparative models are consistent as they all have site class terms, except for ASA14 and Zea18 functions which use continuous V_{S30} measures. In order to plot ASA14 and Zea18 for rock-like site, V_{S30} value of 800 is suggested. BAK11 uses the NEHRP site classification with fairly similar definition to the site classification scheme defined by Iran’s practical building code used here and by SZ16. Since the distance metric used by all comparative models is R_{JB} , the proposed R_{JB} -based model proposed by this study is used.

As shown in Fig. 16, all comparative models have similar shapes and trends over the whole period ranges with V/H peaks locating at very short periods (~ 0.05 s), except at M_w 7 for ASA14 and BAK11 which show small differences at longer periods (~ 0.075 and 0.1 s, respectively). In general, our model predicts the highest V/H spectral ratios at intermediate to long periods compare to other models, except for ASA14 which estimates higher V/H ratios at far distances by a maximum of 18% at $T = 1$ s. According to Fig. 16, the short-period predictions of our proposed model are approximately consistent with Zea18, especially at short distances. Apparently, for $0.7 < T < 2$ s, SZ16 model provides relatively consistent results with our model with minor differences at M_w 5 which shows smooth decreasing trend from 17% at $T = 0.7$ to 6% at $T = 2$ s. SZ16 predictions are not smooth over all period ranges. At $T > 0.4$ s, BAK11 and Zea18 indicates the biggest differences of 40% and 32% respectively with respect to our predictions.

The median V/H estimates from our model follow each other closely for soil and rock site conditions. At short periods ($T < 0.2$ s), our predictions are approximately consistent with other models, while at longer periods, our proposed model predicts notably larger V/H ratios than other comparative models as the differences increases for small-magnitude events. All comparative models exhibit almost flat median V/H predictions for $T < 0.2$ s and for M_w 5 at far distances, while the V/H predictions increase sharply towards longer periods. Generally, V/H ratios are expected to reach their greatest amplitudes at short periods with large magnitude and short distance (Bozorgnia and Campbell 2004). As it is expected, such effect is well pronounced in Fig. 16b as maximum V/H ratios at short period reach as high as 1.2 for R_{JB} 10 km and M_w 7. This value increases for shorter distance or/and larger magnitude.

9 Conclusion

In present study, we developed a prediction model for the ratios of vertical-to-horizontal for 5%-damped response spectral accelerations in the vibration period range of 0.01 to 10 s, PGA and PGV, using Iranian ground-motion database recorded during shallow crustal earthquakes. Proposed models are applicable for the magnitude range of 4.5 to 7.4 and distances of up to 200 km. This broad range of magnitude and distance functionality allows us to prevent extrapolation usually performed for

engineering practical purposes to estimate V/H ratios beyond the valid range of parameters. Four versions of the base functional form are fitted to actual data to explore the most appropriate ones. Among them, two functional forms are selected which both exclude the magnitude-dependent geometric spreading coefficient (b_5 in Eq. 1) and one ignores the magnitude-dependent saturation coefficient as well (b_3 in Eq. 1). Unlike most recently developed models, magnitude saturation effects have been constrained in our models through second-order magnitude term. The selected equations yield unbiased predictions of V/H ratios as a function of explanatory variables of distance, magnitude, site class, and style of faulting. Two main faulting mechanisms of strike–slip and reverse types are employed in the presented functional forms.

We aimed to improve the applicability of the new GMPEs in estimating vertical response spectrums and believe that the new functions could eliminate unnecessary computational effort for assessment of virtual components in practical seismic hazard studies. For this reason, one of the main advances of this research is the development of consistent models based on four distance metrics of point- (R_{epi} and R_{hyp}) and finite-fault (R_{JB} and R_{rup}) models. Compared to four recently developed local and regional V/H models, our proposed models yield the lowermost standard deviations over the whole period range. We verified our models through inspection of between- and within-event residuals analyses and found stable and unbiased trends at all periods, magnitudes, distances, and V_{S30} ranges. The residuals, thus, indicate that the V/H models are consistent with the empirical data.

The V/H estimates appeared to be notably dependent on spectral periods, distance, and site amplification terms. We demonstrate the significant effect of ground type for intermediate-to-long periods. According to our models, higher V/H values are expected at short periods, short distances (at short periods), and rock site condition ($T > 0.2$ s). We conclude that for short spectral periods, the predictions of V/H ratios are more sensitive to distance rather than magnitude.

Acknowledgments The authors acknowledge the Building and Housing Research Center of Iran for permission to access unprocessed ground-motion waveforms used in this study. We are very thankful to the two anonymous reviewers for their constructive comments which helped to improve the quality of the paper, and we acknowledge their contribution with gratitude.

References

- Akkar S, Sandikkaya M, Ay BÖ (2014) Compatible ground-motion prediction equations for damping scaling factors and vertical-to-horizontal spectral amplitude ratios for the broader Europe region. *Bull Earthq Eng* 12:517–547
- Ansari A, Noorzad A, Zare M (2007) Application of wavelet multi-resolution analysis for correction of seismic acceleration records. *J Geophys Eng* 4:1–16
- Ansari A, Noorzad A, Zafarani H, Vahidifard H (2010) Correction of highly noisy strong motion records using a modified wavelet de-noising method. *Soil Dynam Earthq Eng* 30:1168–1181
- Beresnev IA, Nightengale AM, Silva WJ (2002) Properties of vertical ground motions. *Bull Seismol Soc Am* 92:3152–3164
- Bindi D, Luzi L, Massa M, Pacor F (2010) Horizontal and vertical ground motion prediction equations derived from the Italian Accelerometric Archive (ITACA). *Bull Earthq Eng* 8:1209–1230
- Bommer JJ, Akkar S, Kale Ö (2011) A model for vertical-to-horizontal response spectral ratios for Europe and the Middle East. *Bull Seismol Soc Am* 101:1783–1806
- Boore DM (2005) On pads and filters: processing strong motion data. *Bull Seismol Soc Am* 95(2):745–750
- Boore DM, Bommer JJ (2005) Processing of strong-motion accelerograms: needs, options and consequences. *Soil Dynam Earthq Eng* 25:93–115
- Boore DM, Stephens CD, Joyner WB (2002) Comments on baseline correction of digital strong-motion data: examples from the 1999 Hector Mine California, earthquake. *Bull Seismol Soc Am* 92:1543–1560
- Bozorgnia Y, Campbell KW (2004) The vertical-to-horizontal response spectral ratio and tentative procedures for developing simplified V/H and the vertical design spectra. *J Earthq Eng* 8(2):175–207
- Bozorgnia Y, Campbell KW (2016) Ground motion model for the vertical-to-horizontal (V/H) ratios of PGA, PGV, and response spectra. *Earthquake Spectra* 32(2):951–978
- Bozorgnia Y, Niazi M, Campbell KW (1995) Characteristics of free-field vertical ground motion during the Northridge earthquake. *Earthquake Spectra* 11:515–525
- Bozorgnia Y, Niazi M, Campbell KW (1996) Relationship between vertical and horizontal ground motion for the Northridge earthquake. 11th World Conference on Earthquake Engineering, Acapulco, Mexico, Proceedings
- Building and Housing Research Center, BHRC (2005) Iranian code of practice for seismic resistant design of buildings, Standard No. 2800, Third Revision, Building & Housing Research Center, Tehran, Iran (in Persian)
- Cauzzi C, Faccioli E (2008) Broadband (0.05 to 20 s) prediction of displacement response spectra based on worldwide digital records. *J Seismol* 12:453–475
- Darzi A, Zolfaghari MR, Cauzzi C, Fäh D (2018) An empirical ground-motion model for horizontal PGV, PGA and 5%-

- damped elastic response spectra (0.01–10 s) in Iran. *Bull Seismol Soc Am*. <https://doi.org/10.1785/0120180196>
- Edwards B, Poggi V, Fäh D (2011) A predictive equation for the vertical-to-horizontal ratio of ground motion at rock sites based on shear-wave velocity profiles from Japan and Switzerland. *Bull Seismol Soc Am* 101:2998–3019
- Gülerce Z, Abrahamson NA (2011) Site-specific spectra for vertical ground motion. *Earthquake Spectra* 27(4):1023–1047
- Harvard Seismology (2015) Centroid Moment Tensor (CMT) catalog search, www.seismology.harvard.edu/. Last accessed March 2015
- International Seismological Centre (ISC) catalog, <http://www.isc.ac.uk/>. Last accessed March 2015
- Joyner WB, Boore DM (1981) Peak horizontal acceleration and velocity from strong-motion records including records from the 1979 Imperial valley, California, earthquake. *Bull Seismol Soc Am* 71(6):2011–2038
- Joyner WB, Boore DM (1993) Methods for regression analysis of strong-motion data. *Bull Seismol Soc Am* 83:469–487
- Joyner WB, Boore DM (1994) Errata: methods for regression analysis of strong-motion data. *Bull Seismol Soc Am* 84: 955–956
- Kaklamanos J, Baise LG, Boore DM (2011) Estimating unknown input parameters when implementing the NGA ground-motion prediction equations in engineering practice. *Earthquake Spectra* 27:1219–1235
- Kawase H, Aki K (1990) Topography effect at the critical SV-wave incidence: possible explanation of damage pattern by the Whittier Narrows, California, earthquake of 1 October 1987. *Bull Seismol Soc Am* 80:1–30
- National Earthquake Hazards Reduction Program (2009) NEHRP recommended seismic provisions for new buildings and other structures: part 1, provisions, Federal Emergency Management Agency (P-750), BSSC, Building Seismic Safety Council, Washington DC. www.bssconline.org
- National Earthquake Information Center (NEIC) global catalog <https://earthquake.usgs.gov/earthquakes/search/>. Last accessed March 2015
- Poggi V, Edwards B, Fäh D (2012) Characterizing the vertical-to-horizontal ratio of ground motion at soft sediment sites. *Bull Seismol Soc Am* 102:2741–2756
- Scherbaum F, Schmedes J, Cotton F (2004) On the conversion of source-to-site distance measures for extended earthquake source models. *Bull Seismol Soc Am* 94:1053–1069
- Sedaghati F, Pezeshk S (2017) Partially nonergodic empirical ground-motion models for predicting horizontal and vertical PGV, PGA, and 5% damped linear acceleration response spectra using data from the Iranian plateau. *Bull Seismol Soc Am* 107(2):934–948
- Shahvar MP, Zare M, Castellaro S (2013) A unified seismic catalog for the Iranian plateau (1900–2011). *Seismol Res Lett* 84(2):233–249
- Soghrat MR, Ziyaeifar M (2016a) Ground motion prediction equations for horizontal and vertical components of acceleration in northern Iran. *J Seismol* 21(1), 99–125
- Soghrat MR, Ziyaeifar M (2016b) A predictive equation for vertical-to-horizontal response spectral ratios in Northern Iran. *Bull Seismol Soc Am* 106:123–140
- Zafarani H, Luzi L, Lanzano G, Soghrat MR (2018) Empirical equations for the prediction of PGA and pseudo spectral accelerations using Iranian strong-motion data. *J Seismol*: 1–23
- Zolfaghari MR, Darzi A (2014) Design and development of a GIS-based seismo-tectonic source model for Iran. Second European conference on earthquake engineering and seismology (2ECEES), Istanbul, Turkey, 25–29 August 2014
- Zolfaghari MR, Darzi A (2019) Ground-motion models for predicting vertical components of PGA, PGV and 5%-damped spectral acceleration (0.01–10 s) in Iran. *Bull Earthq Eng*. <https://doi.org/10.1007/s10518-019-00623-2>

Publisher's note Springer Nature remains neutral with regard to jurisdictional claims in published maps and institutional affiliations.